RESEARCH ARTICLE

Deep Learning-Based Fault Classification and Location for Underground Power Cable of Nuclear Facilities

ABDELRAHMAN SAID [ID]1, SHERIEF HASHIMA [ID]2, (Senior Member, IEEE), MOSTAFA M. FOUDA [ID]1,3, (Senior Member, IEEE), AND MOHAMED H. SAAD [ID]4

[1]Department of Electrical Engineering, Faculty of Engineering at Shoubra, Benha University, Cairo 11672, Egypt
[2]Engineering Department, Nuclear Research Center (NRC), Egyptian Atomic Energy Authority, Inshas, Cairo 13759, Egypt
[3]Department of Electrical and Computer Engineering, College of Science and Engineering, Idaho State University, Pocatello, ID 83209, USA
[4]Radiation Engineering Department, National Center for Radiation Research and Technology (NCRRT), Egyptian Atomic Energy Authority, Cairo 13759, Egypt

Corresponding author: Sherief Hashima (eng_shrif@yahoo.com)

ABSTRACT Worldwide, Nuclear Power Plants (NPPs) must have higher security protection and precise fault detection systems, especially underground power cable faults, to avoid causing national disasters and keep on safe national ratios of electricity production. Hence, this paper proposes an automatic, effective, and accurate Deep Learning (DL)-based fault classification and location technique for these cables via a One-dimensional Convolutional Neural Network (1D-CNN) and a Binary Support Vector Machine (BSVM). The proposed approach includes four main steps: data collection, feature extraction and reduction, fault detection, and fault classification and location. Signal collection from the underground cable's sending end is performed via the Alternating Transient Program/Electromagnetic Transient Program (ATP/EMTP). Feature extraction and reduction are performed via Fractional Discrete Cosine Transform (FrDCT) and Singular Value Decomposition (SVD) methods. Fault detection is performed through leveraging BSVM with the linear Kernel method in the third step. Finally, this permits 1D-CNN to classify the fault type and locate it. Simulation results confirmed the efficiency of our proposed method, especially for 11kV underground cable faults, including different fault resistances and inception angles. Moreover, the proposed technique is applicable in real-time scenarios with a 99.6% accuracy rate, 0.15sec lowest execution time, and 0.095% maximum error rate for fault location at fractional factor (α) equals to 0.8.

INDEX TERMS Fault location, transient faults, ATP/EMTP, cable, NPP, deep learning, FrDCT, 1D-CNN, BSVM, SVD.

I. INTRODUCTION

According to a report from the World Nuclear Association (WNA), nuclear power contributed to 10.5% of the world's electricity in 2021 [1], [2]. Nuclear Power Plants (NPPs) are among the most critical electrical sources due to their overall merits in the last few years. However, NPPs in distributed networks make the system behave differently than before. Each of these units has affects the system differently upon its characteristics and reactions [3], [4]. Because power cables are often installed under the ground rather than overhead,

The associate editor coordinating the review of this manuscript and approving it for publication was Mohammad Ayoub Khan [ID].

they are minor subjects to outages during adverse weather [5]. Furthermore, due to internal insulation failure or exterior damage, asymmetric and symmetric failures still occur on power networks [6], resulting in a power failure. Real-time surveillance approaches for electrical systems have received much interest in recent years as the reliance on automation increases. Furthermore, due to their functions in interconnecting each piece of electrical equipment, failure diagnostics of cables has become particularly important in the industrial sector [4], [7]–[10]. Therefore, accurate and rapid fault classification and location schemes in the NPP underground power cable are vital for overcoming the entire electric network faults. Such faults might produce hazardous transients, fire,

and explosions due to the cable's excessive heating, equipment failure, and power outages, reducing nuclear system reliability and increasing the possibility of national disaster due to radiation leakage [11]–[13]. Various approaches for measuring fault location in transmission networks have been proposed over the years. However, due to structural variations between the underground cable distribution network and the transmission network, some of the described methodologies cannot be used to find defects in distribution networks [14]. The most well-known fault location approaches include Machine Learning (ML) techniques [15], impedance-based methods [16], traveling wave-based algorithms [17], and state estimation-based approaches [18]. The authors of [12] checked different types of fault location methods and their pros and cons. The study and mining of historical data for predicting the absence or existence of a failure in the power system are known as fault classification. For failure prediction in power systems, pattern recognition approaches and ML algorithms have become crucial [19]. In [13], a new framework based on Deep Learning (DL) that employs a particular type of Recurrent Neural Network (RNN) called Gated Recurrent Unit (GRU) to locate faulty sections in the network is suggested. This study installed intelligent feeder meters in all network nodes, which is its primary disadvantage due to their high cost. The Distribution Networks (DNs) are either radial or ring with underground, overhead, and mixed connections. The sustained faults in DNs affect the connected consumer or customer loads. So far, many fault identifying/locating techniques were reported in the DNs. But when the distributed generators are integrated, the grids keep the system more complex, and the existing protection systems are affected. Ultimately the accuracy of the fault identification techniques is reduced as well. As a result, more accurate fault locating or identifying techniques need to be explored by addressing all the inherent behaviors of the DNs [20], [21]. An advanced signal processing technique called the Stockwell Transform (ST) that combines the advantages of wavelet transform and short-time Fourier Transform (FT) was employed recently to detect and classify faults in distribution grids in [22], but not employed in locating faults and identifying faulty sections in distribution grids. A wideband fault location scheme for distribution systems in distributed generation of different types has been presented and evaluated in [23]. The proposed scheme analyses the system using the high frequency non-fundamental components calculated from the available synchronized and non-synchronized measurements. Distributed Generations (DGs) with non-synchronized measures have been represented by an equivalent impedance over the high-frequency range of interest. But this depends on system parameters. A hybrid signal processing technique (WPT-SVM) combined with a GA-based feature selection method is proposed in [24] for fault location in a distribution line. The presented process acquires one cycle of post-fault voltage and current signal from the sending end of the distribution line under study. In [25], signal processing methods in fault detection in

manufacturing systems are previewed. Still, there are some problems with Discrete Wavelet Transform (DWT) as follows, depending on number of decomposition levels, computational complexity and time (especially for wavelet tree or several decomposition), choosing suitable wavelet type (according to your application), shift sensitivity, poor directionality, and lack of phase information, selecting suitable detail or approximation sub-bands. Short-Time Fourier Transform (STFT) is a simple and powerful time-frequency analysis to describe the instant spectrum of the signal at a specific time, which uses the spectrum of a signal segment centered at that time. However, STFT introduces a poor signal resolution to only describe the static content of the short time segments. Furthermore, Fractional Discrete Cosine Transform (FrDCT) has proved itself as a powerful tool for the analysis of signals by representing rotation of signals in time-frequency plane. The FrDCT, applied in this paper, is a reality-preserving transform, which is derived based on the eigenvalue substitution and eigendecomposition. As shown later, our proposed method provides accurate fault diagnosis results, which is more appropriate for real-time scenarios. Furthermore, the algorithm's efficiency is sustained under a variety of resistance and inception angles. Moreover, it is applicable to any electric power station. However, we focus here on NPP faults due to their extreme importance and safety, which may cause national disasters.

The key contributions of this paper are summarized as follows:

- A novel Deep Learning (DL)-based fault classification and location approach for such cables using a one-dimensional Convolutional Neural Network (1D-CNN) and a Binary Support Vector Machine (BSVM).
- The Alternating Transient Program/Electromagnetic Transient Program (ATP/EMTP) is used to simulate an actual 11kV underground cable connected to an NPP.
- The faulted current response is extracted from the sending end using DL in the fraction domain for various faults and fault conditions.
- FrDCT and Singular Value Decomposition (SVD) methods are used to extract features in the suggested approach. Because of the FrDCT's fractional power parameter, which allows for a spatial-frequency representation of the signal, it is widely employed. As a result, it is possible to use both the spatial and frequency domains.
- SVD is used to minimize the number of features by extracting each phase's most significant singular value. After that, a BSVM and CNN approaches are used to detect, classify, and locate faults using the current training patterns obtained by FrDCT and SVD.
- The fault resistance and inception angles of faults were adjusted to demonstrate the CNN's performance under various fault conditions.

The paper organization is as follows: Section II describes the models of NPP, 11kV underground cable, load, and faults,
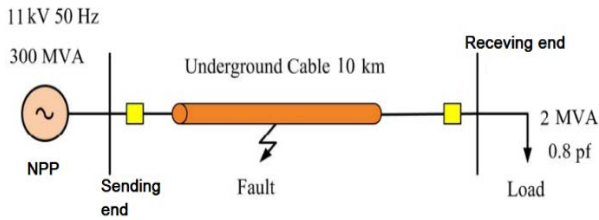
FIGURE 1. The system used in simulation studies, a 10-km three-phase Cross-Linked PolyEthylene (XLPE) stranded copper conductor single-core power cable, and the loading.

respectively. Section III discusses the FrDCT, SVD, SVM, and 1D-CNN mathematical background. Section IV explains the proposed algorithm for fault detection, classification, and location for the system under study. Section V shows ATP/EMTP simulated fault results. The results are shown and discussed in Section VI. Finally, the conclusion is provided in Section VII.

II. SYSTEM MODEL
This section describes the proposed system, the 11kV underground cable, and the utilized NPP model, including the load and different faults.

A. PROPOSED SYSTEM
Fig. 1 shows the system under investigation, where the NPP is connected to the load through the targeted underground cable. The single unit capacity of the NPP is 300MVA, and the load of the plant is 2MVA. The rated terminal voltage is 11kV. NPP detailed data are presented in Table 1 [5], [26]. The phase conductor currents and voltages are defined by a balanced direct-sequence three-phase set of 50Hz sinusoidal currents described in (1), with 106A rms and 8.9kV rms.

$$I_P = 106[1, e^{-j2\frac{\pi}{3}}, e^{j2\frac{\pi}{3}}]A \qquad (1)$$

Because different faults substantially impact nuclear underground cable behavior, it must either be correctly detected or reliably predicted by simulations. This kind of performance necessitates accurate system component modeling. As a result, high-frequency modeling components employing ATP/EMTP are used to create an 11kV Cross-Linked PolyEthylene (XLPE) underground cable connected to NPP.

B. NPP MODEL
The ATP/EMTP model SM59/58 represents the NPP's Synchronous Generator (SG)=300MVA/11kV). Table 1 details the different parameters of SG [5], [26].

C. UNDERGROUND CABLE MODEL
Fig. 2 shows the underground cable type and geometry used in this study. Under identification of dimension and specification of 11kV XLPE underground cable material, where $\mu_c = 1$, $\rho_c = 1.724e^{--8}\Omega.m$ of core conductor, $\mu_{r_1} = \mu_{r_2} = 1$, $\epsilon_{r_1} = \epsilon_{r_2} = 2.7$ of insulation, and $\mu_s = 1$, $\rho_s = 2.84e^{--8}\Omega.m$ of sheath. The cable simulation
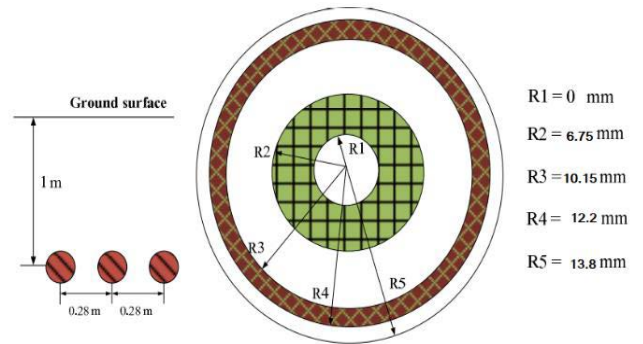

FIGURE 2. The configuration of cable in the simulation study.

(a) (LG)-AG (b) (LL)- AB (c) (LL-G)- AB-G
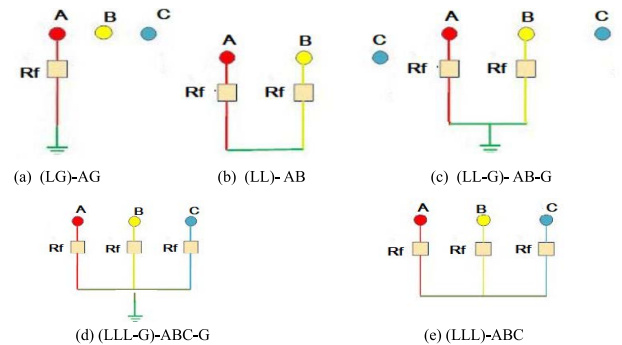
(d) (LLL-G)-ABC-G (e) (LLL)-ABC

FIGURE 3. Asymmetric and symmetric fault types.

was carried out using the Line Cable Conductor Jose Marti (LCC JMarti) model (a frequency-dependent model with constant transformation matrix), also based on traveling wave theory [27]–[30]. where ρ_c is the resistivity of the conductor material. ρ_s refers to the resistivity of the sheath material. μ_c defines the relative permeability of the conductor material. μ_s identifies the relative permeability of the sheath material. μ_r is the relative permeability of the insulating material outside the conductor. ϵ_r is the relative permittivity of the insulating material outside the conductor.

D. LOAD MODELING
A standard component Three-Phase Grounded-Wye load with parallel R, L elements (RLCY3) can easily model the load as a $R = 71.157\omega$ and $L = 365.475mH$ [30].

E. FAULTS MODELING
Based on the kinds indicated in Fig. 3, faults are classed as asymmetric or symmetric. For example, a single-phase to ground fault (Line to Ground (LG)- AG, BG, CG), two-phase fault (Line to Line (LL)- AB, AC, BC), and two-phase fault to the ground ((LL-G)- AB-G, AC-G, BC-G) are all examples of asymmetric faults. On the other hand, three-phase faults, such as three-phase short circuit ((LLL)-ABC) and three-phase short circuit to ground ((LLL-G)-ABC-G), are examples of symmetric faults where A, B, and C signify the system's three phases and G denotes the ground. To explore the influence of varied fault inception angles and fault resistances, short circuits are simulated as a time-controlled switch with resistance in ATP/EMTP [7].

NPP		Underground cable	Positive sequence	Zero sequence	Load	
Voltage (kV)	11		Positive sequence	Zero sequence	Rated (MVA)	2
Short circuit capacity (MVA)	1500	Resistance (Ω/Km)	0.024	0.412		
Resistance (Ω)	14	Inductance (mH/Km)	0.4278	1.533	Power factor	0.85
Inductance (mH)	0.35	Capacitance (µF/Km)	0.2811	0.1529		

III. TERMINOLOGIES

This section will summarize essential feature extraction, reduction, and classification-based techniques. Specifically, we go deep through FrDCT followed by SVD, SVM, and CNN methods.

A. FRACTIONAL DISCRETE COSINE TRANSFORM

The FrDCT is computed based on the Eigen decomposition of the DCT kernel [31]–[33]. The Eigen decomposition of the DCT kernel is obtained using the even Hermite–Gauss eigenvectors of the Fourier matrix D_N^P in the cosine case. The kernel matrix C_N whose element $c_{m,n}$ can be written as:

$$c_{m,n} = \sqrt{\frac{2}{N-1}} k_m k_n cos(\frac{mn\pi}{N-1}), \qquad (2)$$

where m, n = 0,1,...., N - 1 and k_m and k_n are defined as:

$$k_m = \begin{cases} \frac{1}{\sqrt{2}}, & m = 0 \\ 1, & m \neq 0, \end{cases} \qquad k_n = \begin{cases} \frac{1}{\sqrt{2}}, & n = 0 \\ 1, & n \neq 0 \end{cases} \qquad (3)$$

The kernel matrix of FrDCT is mathematically expressed as follows

$$C_{N,\alpha} = C^P = V_N D_N^{\frac{2\alpha}{\pi}} V_{|N}^T$$

$$= V_N \begin{bmatrix} 1 & & & 0 \\ & e^{-2j\alpha} & & \\ & & \ddots & \\ 0 & & & e^{-2j(N-1)\alpha} \end{bmatrix} V_{|N}^T \qquad (4)$$

where N is the number of points, and V_N is the eigenvector derived from k order DFT Hermite eigenvector. The transformed signal is transformed in the frequency domain when α is the fraction factor and equals $\frac{\pi}{2}$. On the other hand, the converted signal is in the time domain when α equals 0. Compared to the DCT, the FrDCT has the order parameter α as an extra degree of freedom. To analyze the faulted phases, time-frequency representations of the FrDCT can be used to enhance the classification rate.

B. SINGULAR VALUE DECOMPOSITION

It is a matrix factorization technique that is extremely useful for various tasks such as pattern recognition, data dimension reduction, matrix approximation, pseudo inverse calculation, and solving linear equations. It can be used to decompose any matrix into three matrices in the following manner:

$$A = U \cdot S \cdot V', \qquad (5)$$

where U and V are unitary matrices, i.e., $UU' = 1$ and $VV' = 1$, that are called left and right singular vectors, respectively. The S matrix is a diagonal matrix representing the singular values of A, which are evaluated by calculating the eigenvalues of AA'. It can be described as follows:

$$S = \begin{pmatrix} S_1 & & & \\ & \cdot & & 0 \\ & & \cdot & \\ 0 & & & S_p \\ & & & & 0 \end{pmatrix} \qquad (6)$$

where ρ is the rank of the matrix A. Note that $s_1 > s_2 > \ldots > s_\rho$

The use of SVD brings its advantages. It can express the feature matrix in several values (singular values), so it is endowed with a dimension reduction strategy. Furthermore, it is more stable against feature changes.

C. SUPPORT VECTOR MACHINE

The optimal separating hyperplane is obtained by maximizing the margin between two or more classes of training data set [34], [35]. This hyperplane lies at the margin's midway and must satisfies

$$Minimize : \frac{1}{2} \|W\|^2 \quad S.T : y_i ((W \cdot C_i + b) \geq 1) \qquad (7)$$

Then the solution to this problem is achieved by optimizing the following equation:

$$E = \frac{1}{2} \| W\|^2 - \sum_i \alpha_i \left(y_i \left(\vec{W} \cdot \vec{V_l} + b \right) - 1 \right) \qquad (8)$$

where W is the set of weights, one for each input feature, y is the output result which indicates the class label ($y \in \{1, -1\}$ for binary classifier), and C is the input features vectors. While V's (called the support vectors) are the selected points from the input training features' data (C) that satisfy the maximum margin above and below the hyper-plane. The output b and α are parameters which determine a unique maximal margin solution. The y's and α's correspond to the selected support vectors V's. The classification of an unknown vector Q is predicted by the decision function $d(Q)$, which is positive for class 1 and negative for class 2 and is defined for the kernel (K) as follows

$$d(Q) = sign \left(\sum_i K(Q, V_i) \right) y_i \alpha_i + b \qquad (9)$$

D. CONVOLUTIONAL NEURAL NETWORKS

CNNs are a form of neural network that has a large number of layers. It analyses grid-structured data and then extracts relevant features. One significant advantage of using CNNs is
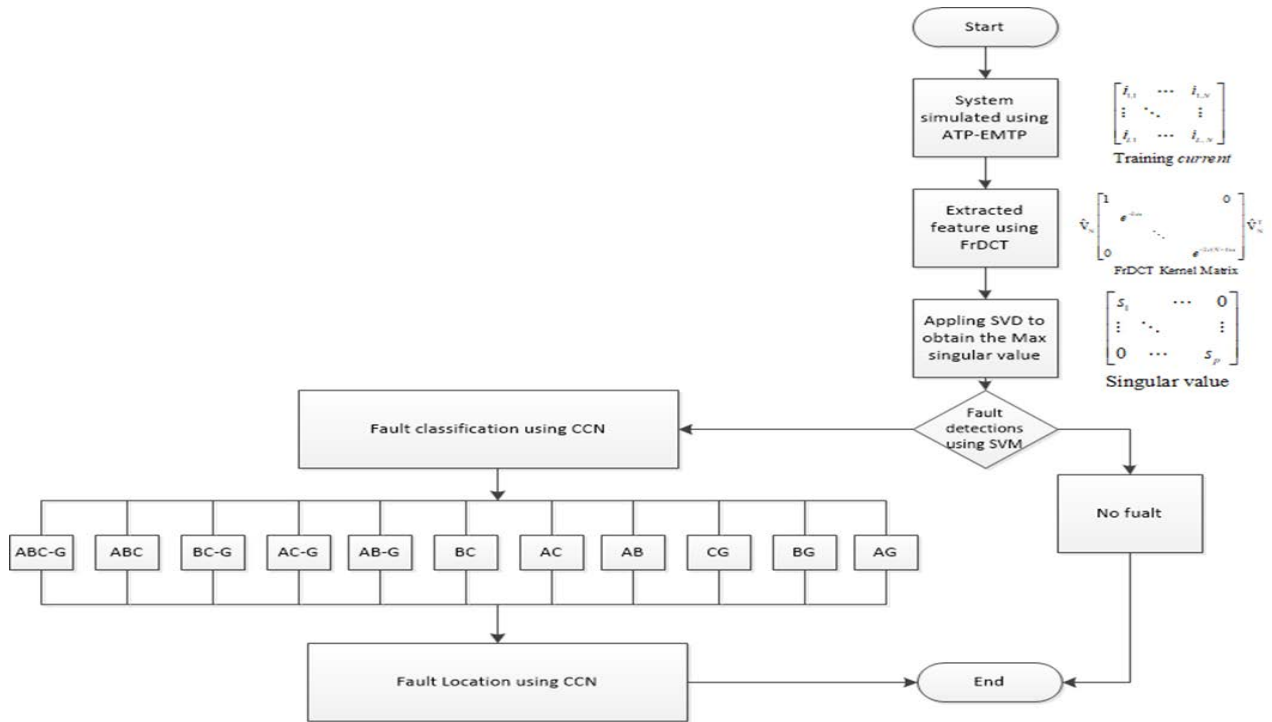
FIGURE 4. Flowchart of the proposed method.
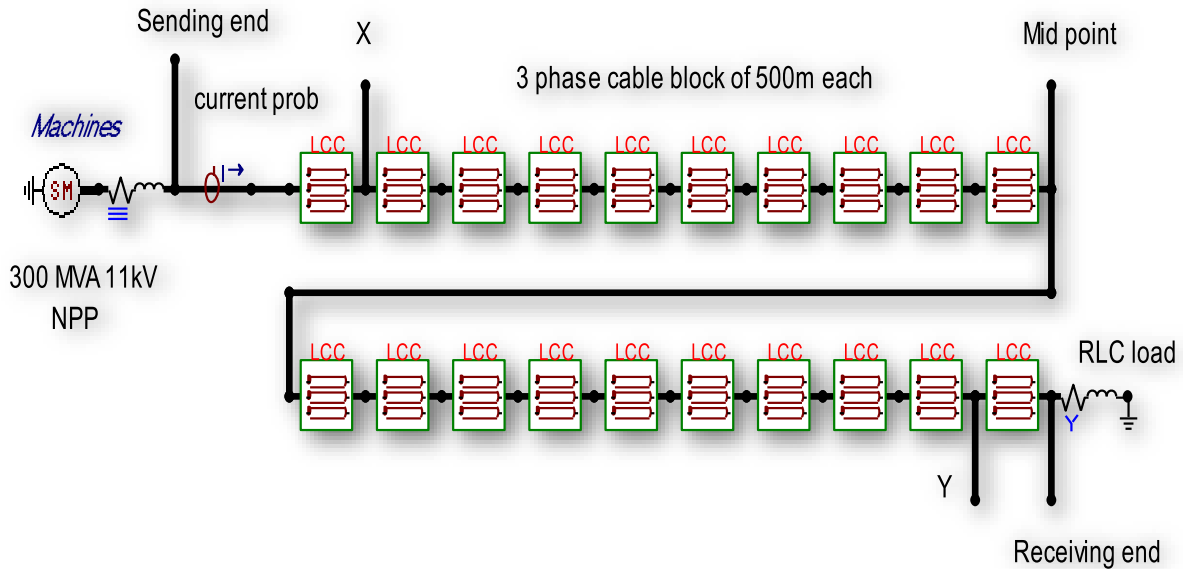
FIGURE 5. Simulated underground cable model.

that no extensive pre-processing is required. 1D-CNNs were introduced in [35] to process 1D data and have been shown to offer numerous computational benefits. Convolution is carried out on data vectors in 1D-CNNs, where an input signal vector x of length N is convolved with a filter vector w of length L. This procedure is stated in 10, resulting in a 1D output layer c with $(NL + 1)$ length without zero padding.

$$c(j) = f\left(\sum_{i=0}^{L-1} w(i) x(j-i) + b\right), \quad j = 0, 1, \cdots, N - p, \tag{10}$$

where b denotes the bias term, and $f(.)$ is a nonlinear function, in this case, the Rectified Linear Unit (ReLU) [35], [36].

Each convolution layer in the proposed architecture is followed by a max pooling layer, in which the maximum value in a kernel window function u of size m×1 and stride s is extracted across an input vector c, resulting in an output vector d defined as:

$$d = max(u(m \times 1, s)c) \tag{11}$$

The Fully Connected (FC) layer takes the feature map generated by the preceding layer as input and connects all of

FIGURE 6. Sending end three-phase current waveforms under regular operation.

(a) AG at (X)

(b) AG at (Y)

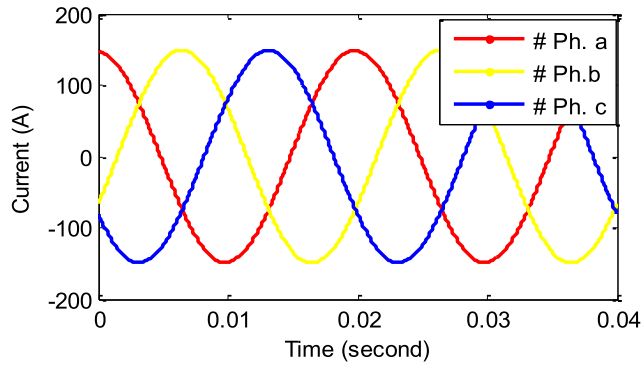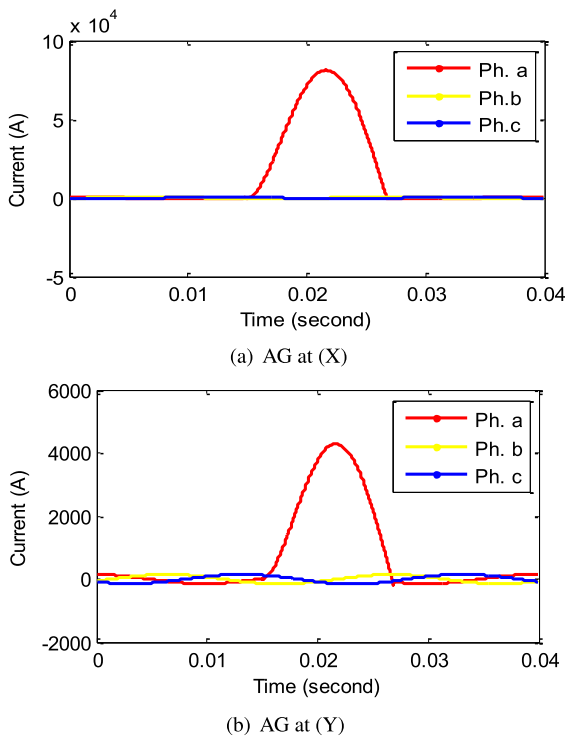**FIGURE 7.** Sending end three-phase current waveforms under AG faults at X, Y points.

TABLE 2. Fault classifier 1D-CNN outputs for various faults.

Fault Type	Phase A	Phase B	Phase C	Ground
AG	1	0	0	1
BG	0	1	0	1
CG	0	0	1	1
AB	1	1	0	0
AC	1	0	1	0
BC	0	1	1	0
AB-G	1	1	0	1
AC-G	1	0	1	1
BC-G	0	1	1	1
ABC	1	1	1	0
ABC-G	1	1	1	1

TABLE 3. Testing results of different network.

Classifier	Time of excution (s)	Performance (%)
PNN [37]	0.514	96.21
kNN [38]	0.683	94.14
RBF [39]	0.411	95.32
Elman [40]	336.214	89.43
MLP [41]	111.138	96.19
FrDCT +SVD+ CNN	0.15	99.6

IV. PROPOSED TECHNIQUE

Herein, we discuss our proposed solution for fault detection, classification, and location based on a deep learning approach. Specifically, BSVM and 1D-CNN techniques for detecting, classifying and locating the fault in underground cables. The BSVM detects if there is faults or not since it is a fast and accurate detection method, especially using linear Kernel with the lowest processing time. If there is a fault, 1D-CNN is utilized to classify and locate such fault. 1D-CNN is utilized due to its high classification accuracy in addition to accurate location with low errors than other methods. The overall processing time for our algorithm is 0.15 s, which is proper to real-time applications.

FrDCT draws intermediate time–frequency representations for a signal. SVD expresses the feature matrix in the form of several values (singular values), so it is endowed a dimension reduction strategy. Furthermore, the singular values have a good stability. One feature is obtained from the maximum SVD of FrDCT for one phase only (max value S matrix). For three-phase underground cable, three features are selected for each fault state.

Figure.4 illustrates different steps of our proposed algorithm in a flow chart structure. It consists of four main stages (input processing, feature extraction&reduction, fault detection, and fault classification & location). The first one processes the obtained current signals from the underground cable's sending end for various fault types and locations. The signals are transformed and reduced in the second stage using FrDCT and SVD to remove the discrimination's dependence on the signal's energy and noise effects, respectively. The FrDCT transformation helps understand and discriminate signal types i.e., feature extraction. SVD assists in obtaining the essential features with high classification accuracy and low processing time. Here, SVD is used due to its low complexity and accurate results. The third stage involves fault detection using BSVM with linear Kernel. The fourth stage includes

the layer's neuron nodes. Batch Normalisation (BN) can be used to normalize and scale the FC layer in order to change its distribution, allowing for faster training. During the network training process, an activation function (such as Softmax, Sigmoid, or others) is used to calculate the expected output, which is then used to calculate the cross-entropy loss l.

$$l = \sum_{k=1} t(k) \log(p(k)) \qquad (12)$$

where C is the number of classes, $t(k)$ denotes the outcome of comparing the predicted label to the ground truth label such that $t(k) = 1$ if the input belongs to class k and 0 otherwise. $p(k)$ denotes the predicted probability that the input belongs to class k. Back propagation is performed using the Adam optimizer [33], which adjusts the network's weights and biases based on the estimated loss.

(a) AB at (X)

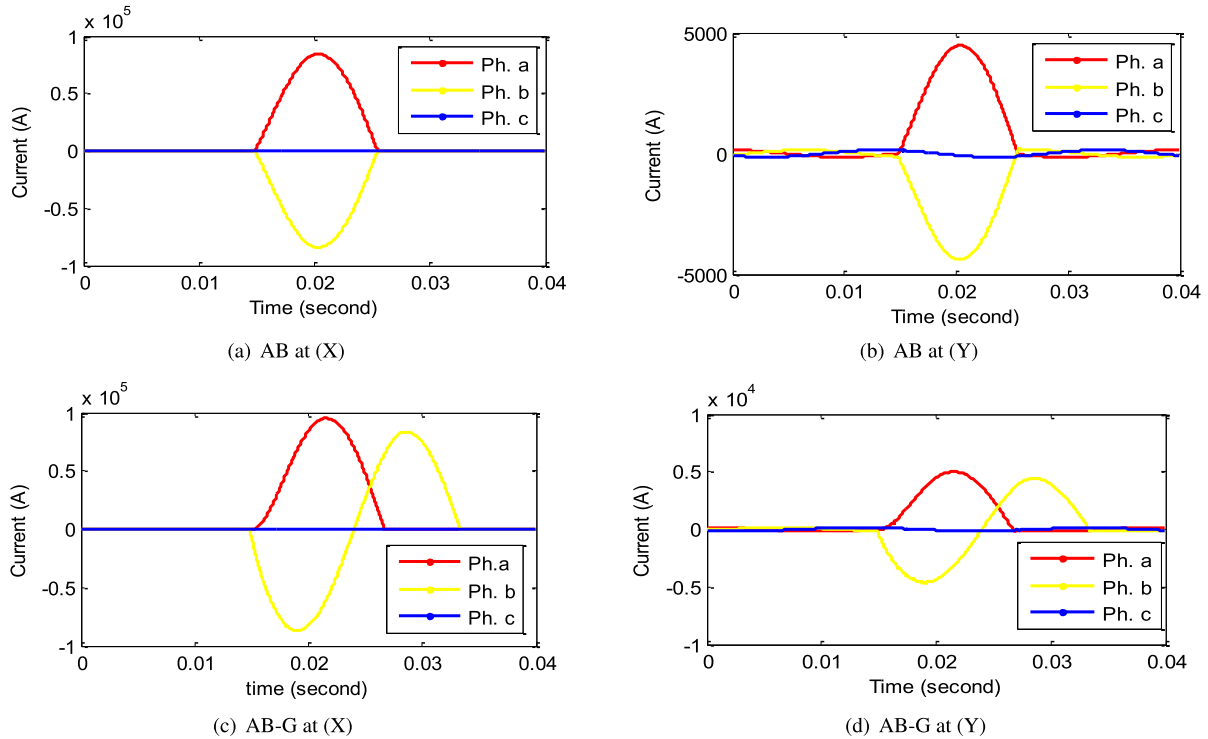(b) AB at (Y)

(c) AB-G at (X)

(d) AB-G at (Y)

FIGURE 8. Sending end three-phase current waveforms under AB,AB-G faults at X, Y points.

faults classification & location using 1D-CNN due to its precise and fast outcomes. As shown in the results and discussion section, the proposed method has efficient performance and is applicable to underground cable fault classification and location problems in real time. The fault location results are precise with variable fault resistance and inception angle.

V. ATP/EMTP SIMULATED FAULT RESULTS

Herein, a practical 11kV underground cable connected to the NPP was used [1]. In addition, a 10-kilometer covert cable model is used in the ATP/EMTP simulation. To create the 10 km underground cable model, twenty identical blocks of 500m in length are cascaded. Fig. 5 shows the designed system. Faults were conducted at the intermediate connections of each subsequent block, with the fault current waveforms being recorded exclusively at the sending end. The four primary fault parameters are fault type, fault distance, fault resistance, and inception angle.

In this respect, eleven types of fault (AG, BG, CG, AB, AC, BC, AB-G, AC-G, BC-G, ABC, ABC-G) and also ten fault resistance in the case of ground short-circuit fault $\mathcal{R} = 0, 20, 50, 75, 100, 125, 150, 175, 200\Omega$), five inception angles Θ° (including 0°, 45°, 90°, 135°,180°) and nineteen distances of fault from recording point (including 500m, 1km,1.5km, 2km, 2.5km, 3km, 3.5km, 4km, 4.5km, 5km, 5.5km, 6km, 6.5km, 7km, 7.5km, 8km, 8.5km, 9km, 9.5km) are simulated. Figs. 5-8 show the sending end three-phase current waveforms after applying various fault types to phases at distances of 500m (cable nearest point to NPP (X)) and at 9.5 km (cable nearest point to load (Y)) from the

source. These faults are applied in 0° degree for the system phases and 0 Ω fault resistance.

Fig. 6 shows the measured sending end current wave's time variation under regular operation. It's clear the current waveform is constant and stable and reaches 150A. Fig. 7 shows the time variation of the measured sending end current wave under LG (AG) at points X and Y. It is noticed that when LG faults occur, the current for the faulted phase is higher compared with the healthy phase. But, the current amplitude for the faulted phase depends on the fault location, which reaches 80 KA and 5 KA when LG is at points X and Y, respectively. When the LL (AB) fault and the LL-G (AB-G) fault occur, the temporal variation of the measured sending end current wave for the faulted phases is larger than for the healthy phases, where phase *A* and phase *B* are substantially higher than phase *C* as shown in Fig. 8.

Fig. 9 shows that when LLL (ABC) fault and LLL-G (ABC-G) occur, the time variation of the measured sending end current wave for the faulted phases is higher than the normal condition. Fig. 10 show the three phase current waveform at sending end under different fault resistance (with fault resistance $\mathcal{R} = 20, 50, 100, 150\Omega$), *InceptionAngle* = 0^0 and fault location=500 m (point X) for the three-phase (a, b, c) to ground fault. It's clear that the faulted phase current amplitude reduced at high value of fault resistance. Fig. 11 show the three phase current waveform at sending end under different inception angle (with $\mathcal{R} = 20\Omega$, Inception Angle = (0°, 45°, 90°, 135°,180°) and fault location=500m (point X) for the three-phase (a, b, c) to ground fault. It's noticed that the initial current amplitude in the case of fault at 45°, 90°, and 135° is much more than 0°, 180°.
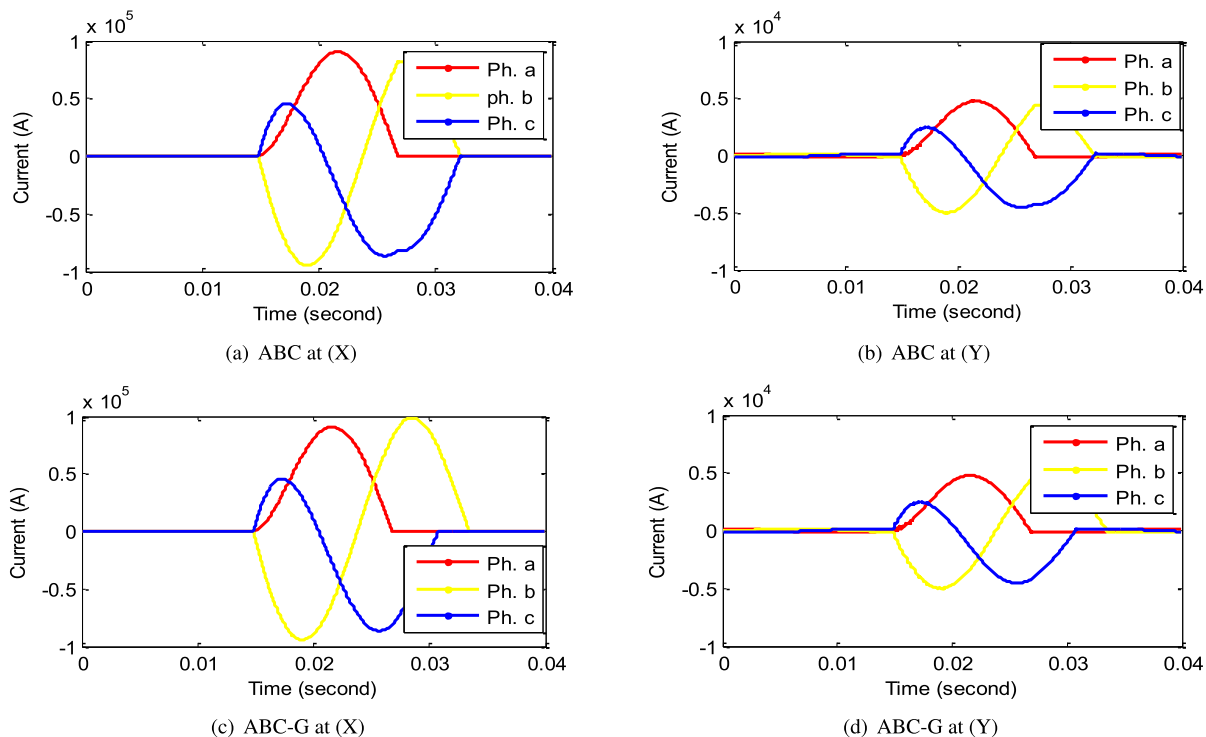
FIGURE 9. Sending end three-phase current waveforms under ABC,ABC-G faults at X, Y points.
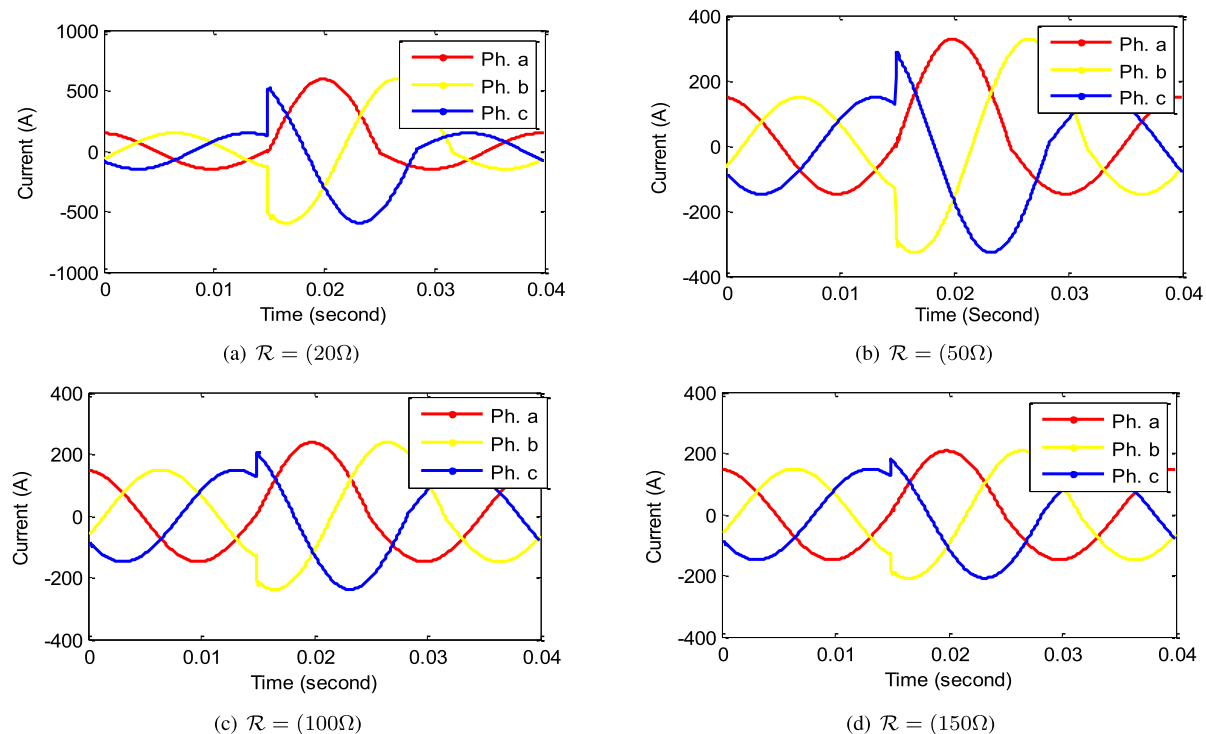
FIGURE 10. Three-phase current waveform at sending end under ABC-G fault with different fault resistance (with fault resistance $\mathcal{R} = (20\Omega, 50\Omega, 100\Omega, 150\Omega)$, $\Theta = 0^o$ and fault location=500m (point X).

VI. RESULTS AND DISCUSSIONS

To illustrate the efficiency of the proposed method eleven types of fault (i.e., AG, BG, CG, AB, AC, BC, AB-G, AC-G, BC-G, ABC, ABC-G) and also ten fault resistances in the case of ground short-circuit fault $\mathcal{R}=0\Omega, 20\Omega, 50\Omega, 75\Omega, 100\Omega, 125\Omega, 150\Omega, 175\Omega, 200\Omega$), five inception angles (including $\Theta = 0°, 45°, 90°, 135°, 180°$) and nineteen distances of fault from recording

(a) $\Theta = 0^{o}$)

(b) $\Theta = 45^{o}$)

(c) $\Theta = 90^{o}$)

(d) $\Theta = 135^{o}$)

(e) $\Theta = 180^{o}$)
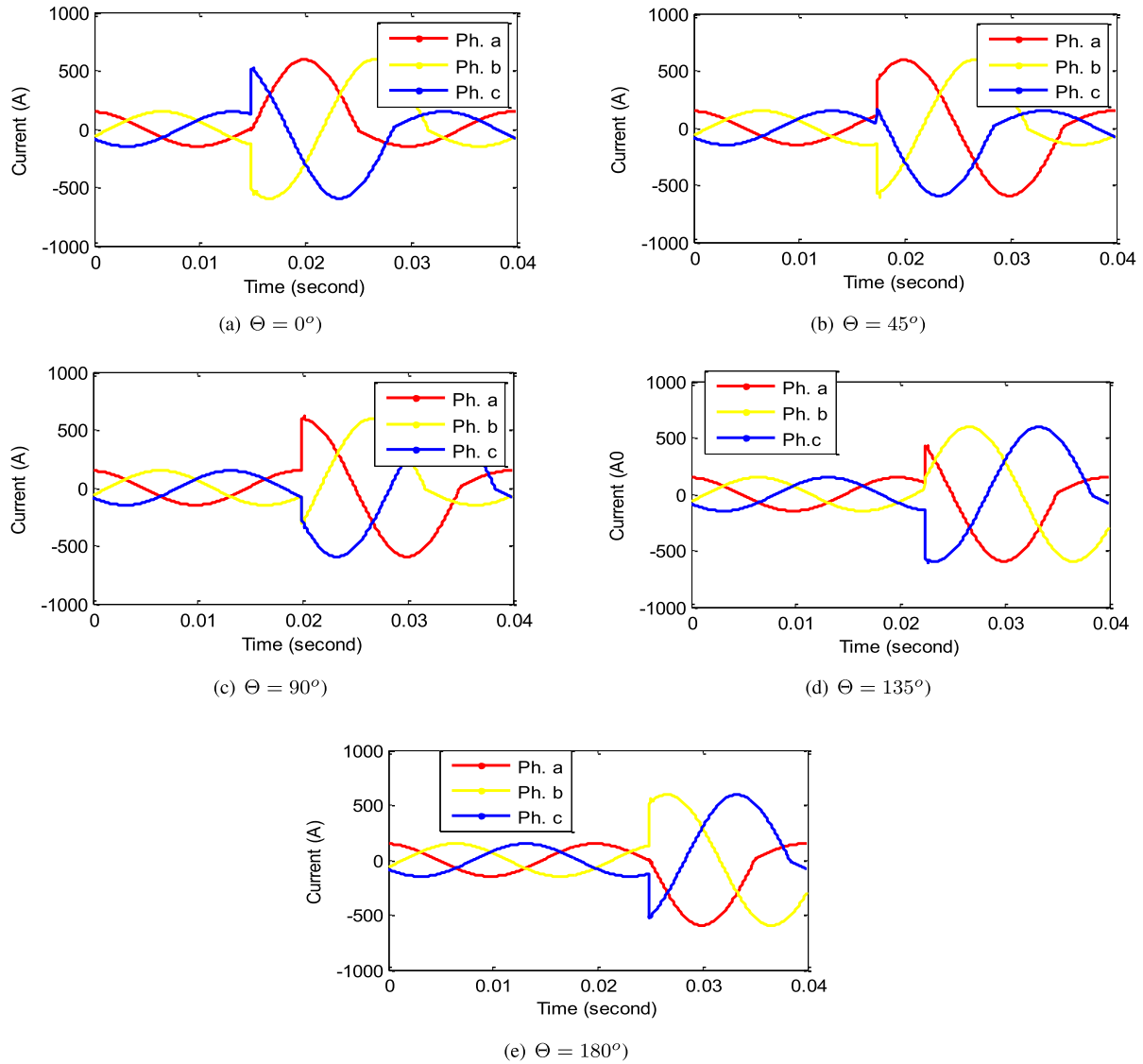
FIGURE 11. Three phase current waveform at sending end under ABC-G fault with different inception angle (with fault resistance $\mathcal{R}20\Omega$, $\Theta = (0°, 45°, 90°, 135°, 180°)$ and fault location=500m (point X).

point (including d=500m, 1km,1.5km, 2km, 2.5km, 3km, 3.5km, 4km, 4.5km, 5km, 5.5km, 6km, 6.5km, 7km, 7.5km, 8km, 8.5km, 9km, 9.5km) are studied. The simulation time is 40 msec with 5 μsec time step, 10 msec fault clearing. Fault type, fault location and fault inception time are changed to obtain training patterns covering a wide range of different power system conditions. In ATP simulation, the sample frequency is about 40 kHz and the transients of only one-terminal phase currents is processed. The data size has 9405 (6584 training and 2822 testing) characteristics for eleven fault types to train and test the 1D-CNN classifier.

This section describes the related results of fault detection using SVM first, followed by classification and location via the CNN approach.

A. FAULT DETECTION USING BSVM
The primary goal is to pinpoint the location of the faulty or the standard cable with pinpoint accuracy. The BSVM classifier

is fed by the outed features of SVD. Its input consists of the maximum value of diagonal S of the SVD of three currents from each phase, which is then normalized. The output of BSVM with linear Kernel is in a straightforward yes or no format, i.e., 1 or 0, which shows whether or not a fault has occurred in the underground cable.

B. FAULT TYPE IDENTIFICATION USING 1D-CNN
As soon as the BSVM detects the cable fault, our next goal is to determine this fault's type using 1D CNN. One feature is obtained from the maximum SVD of FrDCT for one phase only. For three-phase underground cable, three features are selected for each fault state. Therefore, the three-phase feature vector size has 9405 (6584 training and 2822 testing) characteristics for eleven fault types to train and test the 1D-CNN classifier. Table 2 illustrates the truth table describing the flaws and the ideal output for each of the faults.

TABLE 4. Results Of 1D-CNN for 11 faults.

Fault Type	Actual location V(km)	Estimated location U(km)	Error (%)	Fault Type	Actual location (km)	Estimated location (km)	Error (%)
AG	0.5	0.5001	0.0010	BG	0.5	0.50014	0.0014
	1	1.0011	0.0110		1	1.0021	0.021
	1.5	1.5001	0.0010		1.5	1.50071	0.0071
	2	2.0003	0.0030		2	1.999	0.0100
	2.5	2.5004	0.0040		2.5	2.5011	0.0110
	3	2.9995	0.0050		3	3.0034	0.0340
	5	5.0011	0.0110		5	5.0041	0.0410
	7	7.0038	0.0380		7	7.00411	0.04110
	9	9.00513	0.0513		9	9.0071	0.0710
	9.5	9.50781	0.0781		9.5	9.50751	0.0751
CG	0.5	0.5000	00000	AB	0.5	0.50012	0.0012
	1	1.00011	0.0011		1	1.0009	0.009
	1.5	1.50021	0.0021		1.5	1.501	0.01
	2	2.0029	0.0290		2	2.0013	0.013
	2.5	2.50021	0.0021		2.5	2.50015	0.0015
	3	3.0032	0.0320		3	3.0031	0.031
	5	5.00258	0.0258		5	5.00391	0.0391
	7	7.0037	0.0370		7	7.00578	0.0578
	9	9.0058	0.0580		9	9.00614	0.0614
	9.5	9.50598	0.0598		9.5	9.50789	0.0789
AC	0.5	0.5001	0.0010	BC	0.5	0.50011	0.0011
	1	1.00018	0.0018		1	1.0001	0.001
	1.5	1.50021	0.0021		1.5	1.5011	0.011
	2	2.0048	0.0480		2	2.0114	0.114
	2.5	2.50038	0.0038		2.5	2.5009	0.009
	3	3.0029	0.0290		3	3.001	0.010
	5	5.0041	0.0410		5	5.0031	0.031
	7	7.0035	0.0350		7	6.9981	0.0190
	9	9.00687	0.0687		9	9.00412	0.0412
	9.5	9.50711	0.0711		9.5	9.50678	0.0678
AB-G	0.5	0.50014	0.0014	AC-G	0.5	0.50013	0.0013
	1	1.0031	0.0310		1	1.00103	0.0103
	1.5	1.5007	0.0070		1.5	1.50019	0.0019
	2	2.004	0.0400		2	2.0035	0.0350
	2.5	2.50381	0.0381		2.5	2.50024	0.0024
	3	2.9971	0.0290		3	3.00219	0.0219
	5	5.0041	0.0401		5	5.00369	0.0369
	7	7.00514	0.0514		7	7.00458	0.0458
	9	9.05134	0.5134		9	9.00522	0.0522
	9.5	9.50688	0.0688		9.5	9.50671	0.0671
BC-G	0.5	0.5014	0.0140	ABC	0.5	0.50201	0.0201
	1	1.0001	0.0010		1	1.0031	0.0310
	1.5	1.5011	0.0110		1.5	1.50041	0.0041
	2	2.0114	0.1140		2	2.0004	0.0040
	2.5	2.50021	0.0021		2.5	2.50013	0.0013
	3	3.001	0.0100		3	3.0024	0.0240
	5	5.0047	0.0470		5	5.0044	0.0440
	7	7.0018	0.0180		7	7.0054	0.0540
	9	9.0078	0.0780		9	9.0077	0.0770
	9.5	9.50641	0.0641		9.5	9.5071	0.0710
ABC-G	0.5	0.5002	0.0020				
	1	1.0014	0.0140				
	1.5	1.5021	0.0210				
	2	2.0038	0.0380				
	2.5	2.5018	0.0180				
	3	3.0040	0.0400				
	5	4.9990	0.0100				
	7	7.0050	0.0500				
	9	9.00412	0.0412				
	9.5	9.50871	**0.0871**				

C. FAULT CLASSIFICATION

The planned 1D-CNN network consists of 11 inputs and four outputs, one for each of the three phases and one for the ground line. Thus, the outputs are either 0 or 1, indicating the absence or presence of a defect on the appropriate line (A, B, C, or G, where A, B, and C signify the system's three phases and G denotes the ground). Thus, the numerous possible permutations can be used to represent each of the various flaws. Therefore, the suggested 1D-CNN should accurately discriminate between the eleven fault categories. The training set has a total of 9405 input and output patterns (855 for each of the eleven types of errors), each with three inputs and one output. The trained 1D-CNN overall Mean Square Error (MSE) is 0.015002. Moreover, the performance of 1D CNN concerning FrDCT is shown in Fig. 12. The highest performance is 99.6% at a fractional factor (α) of 0.8.

TABLE 5. Results of 1D-CNN for 11 faults $\mathcal{R}$=10 Ω.

Fault Resistance ∇	Fault Type	Actual location V(km)	Estimated location U (km)	Error E (%)
10 Ω	AG	0.5	0.5001	0.0012
		5	5.0021	0.0210
		9.5	9.5079	0.0791
	BG	0.5	0.5011	0.0110
		5	5.0052	0.0520
		9.5	9.5076	0.0762
	CG	0.5	0.5001	0.0010
		5	5.00311	0.0311
		9.5	9.50612	0.0612
	AB	0.5	0.50015	0.0015
		5	5.00411	0.0411
		9.5	9.50797	0.0797
	AC	0.5	0.50021	0.0021
		5	5.00520	0.0520
		9.5	9.50791	0.0791
	BC	0.5	0.50014	0.0014
		5	5.00380	0.0380
		9.5	9.50698	0.0698
	AB-G	0.5	0.50018	0.0018
		5	5.00521	0.0521
		9.5	9.50697	0.0697
	AC-G	0.5	0.50015	0.0015
		5	5.00387	0.0387
		9.5	9.50712	0.0712
	BC-G	0.5	0.50151	0.0151
		5	5.00487	0.0487
		9.5	9.50688	0.0688
	ABC	0.5	0.50212	0.0212
		5	5.00514	0.0514
		9.5	9.50802	0.0802
	ABC-G	0.5	0.50032	0.0032
		5	5.00483	0.0483
		9.5	9.50898	**0.0898**

TABLE 6. Results of 1D-CNN For 11 faults at $\mathcal{R} = 50\Omega$.

Fault Resistance $\mathcal{R}$	Fault Type	Actual location V (km)	Estimated location U(km)	Error E(%)
50 Ω	AG	0.5	0.50017	0.0017
		5	5.00370	0.0370
		9.5	9.50799	0.0799
	BG	0.5	0.50140	0.0140
		5	5.00560	0.0560
		9.5	9.50778	0.0778
	CG	0.5	0.50011	0.0011
		5	5.00354	0.0354
		9.5	9.50634	0.0634
	AB	0.5	0.50016	0.0016
		5	5.00437	0.0437
		9.5	9.50799	0.0799
	AC	0.5	0.500211	0.00211
		5	5.00570	0.05700
		9.5	9.50799	0.0799
	BC	0.5	0.50015	0.0015
		5	5.00397	0.0397
		9.5	9.50731	0.0731
	AB-G	0.5	0.50021	0.0021
		5	5.005381	0.05381
		9.5	9.50699	0.0699
	AC-G	0.5	0.50019	0.0019
		5	5.00398	0.0398
		9.5	9.50717	0.0717
	BC-G	0.5	0.50172	0.0172
		5	5.00489	0.0489
		9.5	9.50695	0.0695
	ABC	0.5	0.50218	0.0218
		5	5.00519	0.0519
		9.5	9.50888	0.0888
	ABC-G	0.5	0.500378	0.00378
		5	5.00488	0.0488
		9.5	9.508982	**0.08982**

TABLE 7. Results of 1D-CNN for 11 faults at $\mathcal{R} = 150\Omega$.

Fault Resistance $\mathcal{R}$	Fault Type	Actual location V(km)	Estimated location U(km)	Error E(%)
150 Ω	AG	0.5	0.50019	0.0019
		5	5.00420	0.0420
		9.5	9.50802	0.0802
	BG	0.5	0.50210	0.0210
		5	5.00610	0.0610
		9.5	9.50798	0.0798
	CG	0.5	0.50180	0.0180
		5	5.003811	0.0381
		9.5	9.50685	0.0685
	AB	0.5	0.50017	0.0017
		5	5.00438	0.0438
		9.5	9.50814	0.0814
	mAC	0.5	0.50022	0.0022
		5	5.00590	0.0590
		9.5	9.50812	0.0812
	BC	0.5	0.50018	0.0018
		5	5.00412	0.0412
		9.5	9.50734	0.0734
	AB-G	0.5	0.50029	0.0029
		5	5.00545	0.0545
		9.5	9.50735	0.0735
	AC-G	0.5	0.50025	0.0025
		5	5.00401	0.0401
		9.5	9.50725	0.0725
	BC-G	0.5	0.5018	0.0180
		5	5.00499	0.0499
		9.5	9.50718	0.0718
	ABC	0.5	0.50299	0.0299
		5	5.00521	0.0521
		9.5	9.50898	0.0898
	ABC-G	0.5	0.50038	0.0038
		5	5.00498	0.0498
		9.5	9.508999	**0.08999**

TABLE 8. Results of 1D-CNN for 11 faults at $\mathcal{R} = 200\Omega$.

Fault Resistance	Fault Type	Actual location V(km)	Estimated location U(km)	Error E(%)
200Ω	AG	0.5	0.50028	0.0028
		5	5.00497	0.0497
		9.5	9.50811	0.0811
	BG	0.5	0.5024	0.0240
		5	5.00632	0.0632
		9.5	9.50843	0.0843
	CG	0.5	0.50210	0.0210
		5	5.00421	0.0421
		9.5	9.50731	0.0731
	AB	0.5	0.5002	0.0020
		5	5.00498	0.0498
		9.5	9.50884	0.0884
	AC	0.5	0.50024	0.0024
		5	5.00612	0.0612
		9.5	9.50834	0.0834
	BC	0.5	0.50019	0.0019
		5	5.00435	0.0435
		9.5	9.50742	0.0742
	AB-G	0.5	0.50034	0.0034
		5	5.00613	0.0613
		9.5	9.50758	0.0758
	AC-G	0.5	0.50029	0.0029
		5	5.00432	0.0432
		9.5	9.50799	0.0799
	BC-G	0.5	0.50211	0.0211
		5	5.00513	0.0513
		9.5	9.50753	0.0753
	ABC	0.5	0.50341	0.0341
		5	5.00529	0.0529
		9.5	9.50899	0.0899
	ABC-G	0.5	0.50045	0.0045
		5	5.00508	0.0508
		9.5	9.5090	**0.0900**

TABLE 9. Results of 1D-CNN for 11 faults at $\Theta = 45^o$.

Inception angle Θ	Fault Type	Actual location V(km)	Estimated location U(km)	Error E(%)
45°	AG	0.5	0.500113	0.00113
		5	5.00130	0.0130
		9.5	9.50783	0.0783
	BG	0.5	0.50014	0.0014
		5	5.0046	0.0460
		9.5	9.50753	0.0753
	CG	0.5	0.50010	0.0010
		5	5.00258	0.0258
		9.5	9.50598	0.0598
	AB	0.5	0.500132	0.0013
		5	5.003910	0.0391
		9.5	9.50789	0.0789
	AC	0.5	0.500141	0.0014
		5	5.00408	0.0408
		9.5	9.50719	0.0719
	BC	0.5	0.50016	0.0016
		5	5.01010	0.1010
		9.5	9.50677	0.0677
	AB-G	0.5	0.50018	0.0018
		5	5.00425	0.0425
		9.5	9.50687	0.0687
	AC-G	0.5	0.50013	0.0013
		5	5.00368	0.0368
		9.5	9.50673	0.06730
	BC-G	0.5	0.50143	0.01430
		5	5.00469	0.04690
		9.5	9.50652	0.06520
	ABC	0.5	0.502081	0.02081
		5	5.00431	0.04310
		9.5	9.50740	0.0740
	ABC-G	0.5	0.50019	0.0019
		5	5.00340	0.0340
		9.5	9.50874	**0.0874**

TABLE 10. Results of 1D-CNN for 11 faults at $\Theta = 90^o$.

Inception angle Θ	Fault Type	Actual location V (km)	Estimated location U(km)	Error E(%)
90°	AG	0.5	0.50012	0.0012
		5	5.0018	0.0180
		9.5	9.50788	0.0788
	BG	0.5	0.50016	0.0016
		5	5.00501	0.0501
		9.5	9.50796	0.0796
	CG	0.5	0.5001	0.0010
		5	5.00289	0.0289
		9.5	9.506452	0.0645
	AB	0.5	0.50018	0.0018
		5	5.00397	0.0397
		9.5	9.50801	0.0801
	AC	0.5	0.50019	0.0019
		5	5.00487	0.0487
		9.5	9.50728	0.0728
	BC	0.5	0.50019	0.0019
		5	5.0107	0.1070
		9.5	9.50685	0.0685
	AB-G	0.5	0.50018	0.0018
		5	5.0045	0.0450
		9.5	9.50697	0.0697
	AC-G	0.5	0.50018	0.0018
		5	5.00378	0.0378
		9.5	9.50689	0.0689
	BC-G	0.5	0.50187	0.0187
		5	5.00498	0.0498
		9.5	9.50678	0.0678
	ABC	0.5	0.50209	0.0209
		5	5.0048	0.0480
		9.5	9.5079	0.0790
	ABC-G	0.5	0.5004	0.0040
		5	5.0035	0.0350
		9.5	9.50899	**0.0899**

TABLE 11. Results of 1D-CNN for 11 faults At $\Theta = 135^o$.

| Inception angle Θ	Fault Type	Actual Location V (km)	Estimated Location U (km)	Error (%) E
135°	AG	0.5	0.500112	0.00112
		5	5.0012	0.012
		9.5	9.50784	0.0784
	BG	0.5	0.50014	0.0014
		5	5.0045	0.045
		9.5	9.50752	0.0752
	CG	0.5	0.5001	0.001
		5	5.00258	0.0258
		9.5	9.50598	0.0598
	AB	0.5	0.500135	0.00135
		5	5.00393	0.0393
		9.5	9.50789	0.0789
	AC	0.5	0.500132	0.0013
		5	5.00402	0.0402
		9.5	9.50719	0.0719
	BC	0.5	0.50015	0.0015
		5	5.0101	0.1010
		9.5	9.50678	0.0678
	AB-G	0.5	0.50016	0.0016
		5	5.00438	0.0438
		9.5	9.50689	0.0689
	AC-G	0.5	0.50012	0.0012
		5	5.00379	0.0379
		9.5	9.50675	0.0675
	BC-G	0.5	0.50151	0.0151
		5	5.00473	0.0473
		9.5	9.50648	0.0648
	ABC	0.5	0.50204	0.0204
		5	5.0043	0.0430
		9.5	9.5074	0.0740
	ABC-G	0.5	0.50025	0.0025
		5	5.0031	0.0310
		9.5	9.50875	**0.0875**
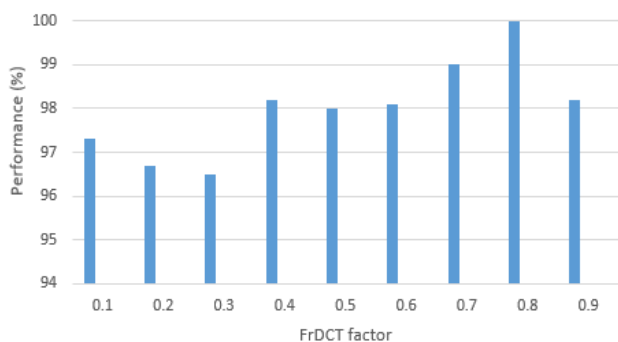
FIGURE 12. The proposed method's performance based on the FrDCT coefficients for different FrDCT factor values.

To evaluate the performance of 1D-CNN, k-nearest neighbour algorithm (kNN) [38], Radial Basis Function networks (RBF) [39], Elman networks [40], Multilayer Perceptrons (MLP) [41], and Probabilistic Neural Networks (PNN) [37] are investigated and compared with our method. The fault classification results using different network structures are shown in Table 3.

As shown in Table 3, the best results were obtained using 1D-CNN, which achieved 99.6% performance levels and required less time than the others because 1D-CNN is trained using only the most significant features than the entire training dataset. Hence, 1D-CNN results in the optimal performance of classification tasks. FrDCT and SVD provides optimal representation of signal by packing most of the information in few coefficients for a given signal. Both MLP and ELMAN take a lot of times because the computations are difficult and time consuming and the proper functioning of the model depends on the quality of the training If the model does not work properly, generalization problems arise.

D. 1D-CNN BASED FAULT LOCATION
After classifying the faulty phases, we initiate our next objective of determining the fault location from the line's sending end. 1D-CNN predicts the actual location of the fault using inputs containing three-phase current data. Numerous fault types have been considered, including 11 faults i.e., AG, BG, CG, AB, AC, BC, AB-G, AC-G, BC-G, ABC, and ABC-G. 1D-CNN was trained and tested using data corresponding to faults occurring at various points along the 10 km underground cable (approximately 20 data points for each case). The distinct high-frequency characteristics of each fault type were determined using FrDCT and SVD. Then, employed to obtain the corrected location of the fault. For each test case, the results were examined to determine the estimation error associated with this test case. The deviation between the estimated fault distance (U) and the actual fault distance (V) for the test case was used to quantify this error, which measures the algorithm's precision. The overall accuracy, E,

TABLE 12. Results of 1D-CNN for 11 faults at $\Theta = 180^o$.

Inception angle Θ	Fault Type	Actual location (km) V	Estimated location (km) U	Error (%) E
180°	AG	0.5	0.50011	0.0011
		5	5.00110	0.0110
		9.5	9.50791	0.0791
	BG	0.5	0.50014	0.0014
		5	5.00420	0.0420
		9.5	9.50751	0.0751
	CG	0.5	0.50010	0.0010
		5	5.00259	0.0259
		9.5	9.50598	0.0598
	AB	0.5	0.50013	0.0013
		5	5.00435	0.0435
		9.5	9.50789	0.0789
	AC	0.5	0.50030	0.0030
		5	5.0044	0.0440
		9.5	9.50715	0.0715
	BC	0.5	0.50012	0.0012
		5	5.01030	0.1030
		9.5	9.50678	0.0678
	AB-G	0.5	0.50015	0.0015
		5	5.00410	0.0411
		9.5	9.50689	0.0689
	AC-G	0.5	0.50015	0.0015
		5	5.00369	0.0369
		9.5	9.50673	0.0673
	BC-G	0.5	0.50160	0.0161
		5	5.00473	0.0473
		9.5	9.50651	0.0651
	ABC	0.5	0.50205	0.0205
		5	5.00450	0.0450
		9.5	9.50740	0.074
	ABC-G	0.5	0.50023	0.0023
		5	5.00300	0.0300
		9.5	9.50874	**0.0874**

TABLE 13. Results of 1D-CNN for 11 faults at $\mathcal{R} = 200\Omega$ and $= 90^o$.

Inception angle Θ	Fault Resistance $\mathcal{R}$	Fault Type	Actual location V (km)	Estimated location U (km)	Error (%) E
90°	200Ω	AG	9.5	9.507010	0.07010
		BG	9.5	9.507231	0.07231
		CG	9.5	9.50735	0.07350
		AB	9.5	9.50751	0.0751
		AC	9.5	9.50789	0.0789
		BC	9.5	9.50711	0.0711
		AB-G	9.5	9.50720	0.0720
		AC-G	9.5	9.50773	0.0773
		BC-G	9.5	9.50725	0.0725
		ABC	9.5	9.50820	0.0820
		ABC-G	9.5	9.50950	**0.0950**

can be expressed as the maximum estimation error across the entire length range of the cable for all possible fault types expressed as a percentage of the total cable length C.

$$E = \frac{U - V}{C} X 100 \qquad (13)$$

The testing results are presented in Table 4, which shows that the maximum percentage error in locating the fault is limited to (0.0871% of L) kms in the worst-case scenario. The greatest estimation errors occur at the receiving end of the cable's closest points. Similar results have been obtained for other types of faults and system conditions in terms of fault location accuracy. Additionally, different values of fault resistances $\mathcal{R}$ and inception angles Θ are tested to evaluate the 1D-CNN's performance under numerous operating conditions. Tables 5-8 show faults' actual and predicted locations at 10 Km with various fault resistances at constant

$\Theta = 0 (\mathcal{R} = 10, \mathcal{R} = 50, \mathcal{R} = 150, \mathcal{R} = 200$, respectively). The worst case was found at $\mathcal{R} = 200$, i.e., Table 8. Variable fault resistance values have no effect on accurate classification of fault location as shown in the tables.

Tables 9-12 show faults' actual and estimated locations at 10 Km with various fault resistance at no fault resistance ($\Theta = 45^o$, $\Theta = 90^o$, $\Theta = 135^o$, $\Theta = 180^o$, respectively). The worst case is at $\Theta = 90^o$ Table 10. The tables confirm the accurate classification of fault locations at different inception angles.

Table 13 illustrates faults' actual and estimated locations of 10 Km underground cable at $\mathcal{R} = 200$ and $\Theta = 90^o$, i.e. worst case. The location of the fault, the fault resistance value, and inception angle have no effect on the accuracy of fault location. The maximum error (0.095%) in fault location occurs when the $\mathcal{R} = 200\Omega$ and $\Theta = 90^o$ at the cable receiving end (9.5 km). Simulation results confirm that 1D-CNN

combined with FrDCT and SVD is an efficient method for locating fault in practical 11kV underground cable connected to NPP. The proposed method can determine the fault location easily, quickly, and accurately under different conditions.

VII. CONCLUSION

Fault detections of underground cables are vital, especially for those fed NPPs. This paper presented a DL-based fault classification and location technique in NPP three-phase underground power cables. First, ATP/EMTP simulator models several fault types with variable locations under variable settings to feed such data to our proposed method. Then, the proposed technique optimized the performances of fault classification, location, and execution time by combining FrDCT with SVD, BSVM, and 1D-CNN, respectively. Simulation results confirmed the superior performance of the proposed technique regards detecting, classifying, and locating faults effectively, quickly (0.15sec), and accurately (maximum error between 1D-CNN output and actual output is 0.095%). Hence, our proposed method could be used as a part of a new generation of high-speed advanced fault locators. Future work will include inspection of our planned model in a realistic power system network.

REFERENCES

[1] L. Wang, W. Sun, J. Zhao, and D. Liu, "A speed-governing system model with over-frequency protection for nuclear power generating units," *Energies*, vol. 13, no. 1, p. 173, Dec. 2019. [Online]. Available: https://www.mdpi.com/1996-1073/13/1/173

[2] *World Nuclear Performance Report 2021*. Accessed: May 22, 2022. [Online]. Available: https://world-nuclear.org/our-association/publications/global-trends-reports/world-nuclear-performance-report.aspx

[3] Y. Ohki and N. Hirai, "Fault location in a cable for a nuclear power plant by frequency domain reflectometry," in *Proc. Int. Conf. Condition Monit. Diagnosis (CMD)*, Sep. 2016, pp. 36–39.

[4] H. Lim, G.-Y. Kwon, and Y.-J. Shin, "Fault detection and localization of shielded cable via optimal detection of time–frequency-domain reflectometry," *IEEE Trans. Instrum. Meas.*, vol. 70, pp. 1–10, 2021.

[5] K. Zhu and P. W. T. Pong, "Fault classification of power distribution cables by detecting decaying DC components with magnetic sensing," *IEEE Trans. Instrum. Meas.*, vol. 69, no. 5, pp. 2016–2027, May 2020.

[6] S. C. Chu, "Screening factor of pipe-type cable systems," *IEEE Trans. Power App. Syst.*, vol. PAS-88, no. 5, pp. 522–528, May 1969.

[7] A. H. I. Mansour, "Fault detection in underground cables by using wavelet technique (WT)," *J. Al-Azhar Univ. Eng. Sector*, vol. 13, no. 48, pp. 1004–1014, Jul. 2018.

[8] A. Ngaopitakkul, C. Pothisarn, and M. Leelajindakrairerk, "Study of characteristics for simultaneous faults in distribution underground cable using DWT," in *Proc. IEEE Region 10 Conf. (TENCON)*, Nov. 2011, pp. 1375–1378.

[9] A. H. A. Bakar, M. S. Ali, C. Tan, H. Mokhlis, H. Arof, and H. A. Illias, "High impedance fault location in 11 kV underground distribution systems using wavelet transforms," *Int. J. Electr. Power Energy Syst.*, vol. 55, pp. 723–730, Feb. 2014. [Online]. Available: https://www.sciencedirect.com/science/article/pii/S0142061513004195

[10] X. Hu, H. Zhang, D. Ma, and R. Wang, "A tnGAN-based leak detection method for pipeline network considering incomplete sensor data," *IEEE Trans. Instrum. Meas.*, vol. 70, pp. 1–10, 2021.

[11] S. P. Nowlen, "Cable failure modes and effects risk analysis perspectives," in *Probabilistic Safety Assessment and Management*, C. Spitzer, U. Schmocker, and V. N. Dang, Eds. London, U.K.: Springer, 2004, pp. 2481–2486.

[12] R. Dashti, M. Daisy, H. Mirshekali, H. R. Shaker, and M. H. Aliabadi, "A survey of fault prediction and location methods in electrical energy distribution networks," *Measurement*, vol. 184, Nov. 2021, Art. no. 109947. [Online]. Available: https://www.sciencedirect.com/science/article/pii/S0263224121008824

[13] M. R. Shadi, H. Mirshekali, R. Dashti, M.-T. Ameli, and H. R. Shaker, "A parameter-free approach for fault section detection on distribution networks employing gated recurrent unit," *Energies*, vol. 14, no. 19, p. 6361, Oct. 2021. [Online]. Available: https://www.mdpi.com/1996-1073/14/19/6361

[14] A. S. Ghoniem, "Sub-line transient magnetic fields calculation approach for fault detection, classification and location of high voltage transmission line," *Int. J. Electr. Eng. Informat.*, vol. 11, no. 3, pp. 548–563, Sep. 2019.

[15] S. Rahman Fahim, S. K. Sarker, S. M. Muyeen, M. R. I. Sheikh, and S. K. Das, "Microgrid fault detection and classification: Machine learning based approach, comparison, and reviews," *Energies*, vol. 13, no. 13, p. 3460, Jul. 2020. [Online]. Available: https://www.mdpi.com/1996-1073/13/13/3460

[16] H. Mirshekali, R. Dashti, and H. R. Shaker, "An accurate fault location algorithm for smart electrical distribution systems equipped with micro phasor mesaurement units," in *Proc. Int. Symp. Adv. Electr. Commun. Technol. (ISAECT)*, Nov. 2019, pp. 1–7.

[17] Y. Shi, T. Zheng, and C. Yang, "Reflected traveling wave based single-ended fault location in distribution networks," *Energies*, vol. 13, no. 15, p. 3917, 2020. [Online]. Available: https://www.mdpi.com/1996-1073/13/15/3917

[18] Y. Liu, A. P. S. Meliopoulos, Z. Tan, L. Sun, and R. Fan, "Dynamic state estimation-based fault locating on transmission lines," *IET Gener., Transmiss. Distrib.*, vol. 11, no. 17, pp. 4184–4192, Nov. 2017. [Online]. Available: https://digital-library.theiet.org/content/journals/10.1049/iet-gtd.2017.0371

[19] S. Zhang, Y. Wang, M. Liu, and Z. Bao, "Data-based line trip fault prediction in power systems using LSTM networks and SVM," *IEEE Access*, vol. 6, pp. 7675–7686, 2018.

[20] A. M. I. Haleem, M. Sharma, K. S. Sajan, and K. N. D. Babu, "A comparative review of fault location/identification methods in distribution networks," in *Proc. 1st Int. Conf. Adv. Res. Eng. Sci. (ARES)*, Jun. 2018, pp. 1–6.

[21] M. Shafiullah, M. Abido, and T. Abdel-Fattah, "Distribution grids fault location employing ST based optimized machine learning approach," *Energies*, vol. 11, no. 9, p. 2328, Sep. 2018. [Online]. Available: https://www.mdpi.com/1996-1073/11/9/2328

[22] Y. Yu, M. Li, T. Ji, and Q. H. Wu, "Fault location in distribution system using convolutional neural network based on domain transformation," *CSEE J. Power Energy Syst.*, vol. 7, no. 3, pp. 472–484, 2021.

[23] F. Aboshady, D. Thomas, and M. Sumner, "A fault location scheme for active untransposed distribution systems using a limited number of synchronized measurements," *Electr. Power Compon. Syst.*, vol. 48, nos. 1–2, pp. 1–11, Jan. 2020, doi: 10.1080/15325008.2020.1731880.

[24] P. Ray and D. P. Mishra, "Signal processing technique based fault location of a distribution line," in *Proc. IEEE 2nd Int. Conf. Recent Trends Inf. Syst. (ReTIS)*, Jul. 2015, pp. 440–445.

[25] Z. Germán-Salló and G. Strnad, "Signal processing methods in fault detection in manufacturing systems," *Proc. Manuf.*, vol. 22, pp. 613–620, 2018. [Online]. Available: https://www.sciencedirect.com/science/article/pii/S2351978918303858

[26] R. Cole and R. Tuck, "Bus differential protection upgrade for a 1,500 MVA nuclear power plant with atypical connections," in *Proc. 75th Annu. Georgia Tech Protective Relaying Conf.*, Atlanta, GA, USA, 2022, pp. 1–12.

[27] A. Said, "Analysis of 500 kV OHTL polluted insulator string behavior during lightning strokes," *Int. J. Electr. Power Energy Syst.*, vol. 95, pp. 405–416, Feb. 2018. [Online]. Available: https://www.sciencedirect.com/science/article/pii/S0142061517310281

[28] E. M. T. Eldin, M. I. Gilany, M. M. Abdelaziz, and D. K. Ibrahim, "An accurate fault location scheme for connected aged cable lines in double-fed systems," *Int. J. Electr. Eng.*, vol. 88, no. 5, pp. 431–439, 2006, doi: 10.1007/s00202-005-0299-x.

[29] A. Rafinia and J. Moshtagh, "A new approach to fault location in three-phase underground distribution system using combination of wavelet analysis with ANN and FLS," *Int. J. Electr. Power Energy Syst.*, vol. 55, pp. 261–274, Feb. 2014. [Online]. Available: https://www.sciencedirect.com/science/article/pii/S0142061513003931

[30] M. B. Eteiba, W. I. Wahba, and S. Barakat, "ANFIS approach for locating faults in underground cables," *Int. J. Electr. Comput. Eng.*, vol. 8, no. 6, pp. 905–910, 2014. [Online]. Available: https://publications.waset.org/vol/90

[31] G. Cariolaro, T. Erseghe, and P. Kraniauskas, "The fractional discrete cosine transform," *IEEE Trans. Signal Process.*, vol. 50, no. 4, pp. 902–911, Apr. 2002.

[32] S.-C. Pei and M.-H. Yeh, "The discrete fractional cosine and sine transforms," *IEEE Trans. Signal Process.*, vol. 49, no. 6, pp. 1198–1207, Jun. 2001.

[33] I. Venturini and P. Duhamel, "Reality preserving fractional transforms [signal processing applications]," in *Proc. IEEE Int. Conf. Acoust., Speech, Signal Process.*, vol. 5, May 2004, p. 205.

[34] M. Awad and R. Khanna, *Efficient Learning Machines: Theories, Concepts, and Applications for Engineers and System Designers*, 1st ed. New York, NY, USA: Apress, 2015.

[35] S. Tong and D. Koller, "Support vector machine active learning with applications to text classification," *J. Mach. Learn. Res.*, vol. 2, pp. 45–66, Mar. 2002, doi: 10.1162/153244302760185243.

[36] L. Eren, T. Ince, and S. Kiranyaz, "A generic intelligent bearing fault diagnosis system using compact adaptive 1D CNN classifier," *J. Signal Process. Syst.*, vol. 91, no. 2, pp. 179–189, Feb. 2019, doi: 10.1007/s11265-018-1378-3.

[37] A. Ngaopitakkul and N. Suttisinthong, "Discrete wavelet transform and probabilistic neural network algorithm for classification of fault type in underground cable," in *Proc. Int. Conf. Mach. Learn. Cybern.*, Jul. 2012, vol. 1, no. 2, pp. 360–366.

[38] A. A. Majd, H. Samet, and T. Ghanbari, "K-NN based fault detection and classification methods for power transmission systems," *Protection Control Mod. Power Syst.*, vol. 2, no. 1, Dec. 2017, Art. no. 32.

[39] W.-M. Lin, C.-D. Yang, J.-H. Lin, and M.-T. Tsay, "A fault classification method by RBF neural network with OLS learning procedure," *IEEE Trans. Power Del.*, vol. 16, no. 4, pp. 473–477, Oct. 2001.

[40] S. Ekici, S. Yildirim, and M. Poyraz, "A transmission line fault locator based on Elman recurrent networks," *Appl. Soft Comput.*, vol. 9, no. 1, pp. 341–347, Jan. 2009. [Online]. Available: https://www.sciencedirect.com/science/article/pii/S1568494608000732

[41] A. N. Hasan, P. S. P. Eboule, and B. Twala, "The use of machine learning techniques to classify power transmission line fault types and locations," in *Proc. Int. Conf. Optim. Electr. Electron. Equip. (OPTIM), Int. Aegean Conf. Electr. Mach. Power Electron. (ACEMP)*, May 2017, pp. 221–226.

SHERIEF HASHIMA (Senior Member, IEEE) received the B.Sc. degree (Hons.) in electronics and communication engineering (ECE) from Tanta University, in 2004, the M.Sc. degree (Hons.) in electronics and communication engineering (ECE) from Menoufiya University, Egypt, in 2010, and the Ph.D. degree from the Egypt-Japan University of Science & Technology (EJUST), Alexandria, Egypt, in 2014. He has been working as an Associate Professor at the Engineering and Scientific Equipment Department, Nuclear Research Center (NRC), Egyptian Atomic Energy Authority (EAEA), Egypt, since 2014. From January 2018 to June 2018, he was a Visiting Researcher at the Center for Japan-Egypt Cooperation in Science and Technology, Kyushu University. He has been a Postdoctoral Researcher with the Computational Learning Theory Team, RIKEN AIP, Japan, since July 2019. His research interests include wireless communications, machine learning, online learning, 5G, B5G, 6G systems, image processing, millimeter waves, nuclear instrumentation, and the Internet of Things. He is a technical committee member in many international conferences and a reviewer in many international conferences, journals, and transactions. He is a member of AAAI.

MOSTAFA M. FOUDA (Senior Member, IEEE) received the Ph.D. degree in information sciences from Tohoku University, Japan, in 2011. He worked as an Assistant Professor with Tohoku University, Japan. He was a Postdoctoral Research Associate with Tennessee Technological University, Cookeville, TN, USA. He is currently an Assistant Professor with the Department of Electrical and Computer Engineering, Idaho State University, Idaho Falls, ID, USA. He also holds the position of an Associate Professor with Benha University, Egypt. He has more than 90 publications in international conferences, journal articles, and book chapters. His research interests include cyber security, machine learning, blockchain, the IoT, 6G networks, smart healthcare, and smart grid communications. He has served on the technical committees for several IEEE conferences. He is also a reviewer in several IEEE TRANSACTIONS and Magazines. He is an Editor of the IEEE TRANSACTIONS ON VEHICULAR TECHNOLOGY (TVT) and an Associate Editor of IEEE ACCESS.

ABDELRAHMAN SAID was born in Cairo, Egypt, in March 1987. He received the B.Sc. degree (Hons.) in electrical power and machines, and the M.Sc. and Ph.D. degrees in high voltage engineering from the Electrical Power and Machines Department, Faculty of Engineering at Shoubra, Benha University, Cairo, Egypt, in 2009, 2013, and 2016, respectively. He is currently an Associate Professor with the Electrical Engineering Department, Faculty of Engineering at Shoubra, Benha University. His research interests include transient phenomenon in power networks, artificial intelligent in power systems, and renewable energy.

MOHAMED H. SAAD was born in Egypt, in 1982. He received the B.Sc. degree (Hons.) in communication and electronics engineering from Benha University, Egypt, in 2004, and the M.Sc. and Ph.D. degrees in communication and electronics engineering from Al-Azhar University, Egypt, in 2010 and 2013, respectively. Since 2006, he has been with the Radiation Engineering Department, Atomic Energy Authority, Cairo, Egypt, where he is currently an Associate Professor. His main research interests include image and signal processing, FPGA, GPU, as well as simulation and modeling.

• • •